Transportation Research Part B 150 (2021) 524–539

Contents lists available at ScienceDirect

Transportation Research Part B

journal homepage: www.elsevier.com/locate/trb

Calibration of stochastic link-based fundamental diagram with explicit consideration of speed heterogeneity

Lu Bai [a], S.C. Wong [a,*], Pengpeng Xu [a], Andy H.F. Chow [b], William H.K. Lam [c]

[a] Department of Civil Engineering, The University of Hong Kong, Pokfulam Road, Hong Kong, China
[b] Department of Architecture and Civil Engineering, City University of Hong Kong, Tat Chee Avenue, Hong Kong, China
[c] Department of Civil and Environmental Engineering, The Hong Kong Polytechnic University, Yuk Choi Road, Hong Kong, China

ARTICLE INFO

Keywords:
Speed heterogeneity
Stochastic link-based fundamental diagram
Random-parameter model
Bayesian hierarchical model
Rainfall intensity

ABSTRACT

This study aims to establish a stochastic link-based fundamental diagram (FD) with explicit consideration of two available sources of uncertainty: speed heterogeneity, indicated by the speed variance within an interval, and rainfall intensity. A stochastic structure was proposed to incorporate the speed heterogeneity into the traffic stream model, and the random-parameter structures were applied to reveal the unobserved heterogeneity in the mean speeds at an identical density. The proposed stochastic link-based FD was calibrated and validated using real-world traffic data obtained from two selected road segments in Hong Kong. Traffic data were obtained from the Hong Kong Journey Time Indication System operated by the Hong Kong Transport Department during January 1 to December 31, 2017. The data related to rainfall intensity were obtained from the Hong Kong Observatory. A two-stage calibration based on Bayesian inference was proposed for estimating the stochastic link-based FD parameters. The predictive performances of the proposed model and three other models were compared using *K*-fold cross-validation. The results suggest that the random-parameter model considering the speed heterogeneity effect performs better in terms of both goodness-of-fit and predictive accuracy. The effect of speed heterogeneity accounts for 18%–24% of the total heterogeneity effects on the variance of FD. In addition, there exists unobserved heterogeneity across the mean speeds at an identical density, and the rainfall intensity negatively affects the mean speed and its effect on the variance of FD differs at different densities.

1. Introduction

The fundamental diagram (FD), which aims to establish a fundamental relationship among traffic speed, traffic density, and traffic flow, forms the basis of traffic flow theory. Since the introduction of the linear speed–density relationship by Greenshields et al. (1935), its mathematic formulations have been extensively improved (Del Castillo and Benitez, 1995; Greenberg, 1959; Ji et al., 2010; Kerner, 2004; Lighthill and Whitham, 1955; Newell, 1961; Pipes, 1967; Richards, 1956; Underwood, 1961; Van Aerde, 1995). These relationships can be either established empirically or derived using microscopic models. Further improvements have been made to decompose a single model into multiple models to better fit the empirical data (Drake et al., 1967; Edie, 1961; May, 1990; Wang et al.,

* Corresponding author.
E-mail addresses: xinyuesther@126.com (L. Bai), hhecwsc@hku.hk (S.C. Wong), pengpengxu@yeah.net (P. Xu), andychow@cityu.edu.hk (A.H.F. Chow), william.lam@polyu.edu.hk (W.H.K. Lam).

https://doi.org/10.1016/j.trb.2021.06.021
Received 4 January 2021; Received in revised form 15 May 2021; Accepted 29 June 2021
Available online 15 July 2021

2011; Wu, 2002; Zhang and Kim, 2005). Multi-regime models divide the entire traffic flow into multiple relatively homogeneous traffic conditions, for each of which a specific curve is fitted to represent a distinct traffic condition.

Both single- and multi-regime models establish an equilibrium speed–density relationship under a strong hypothesis that each density corresponds to only one deterministic value of mean speed. This relationship, however, very likely fails to hold in reality due to the existence of inherent uncertainty in macroscopic traffic flow (Qu et al., 2017; Siqueira et al., 2016). Different drivers have different perceptions and responses in various traffic environments and road conditions, which results in different average speeds. Even a population of identical driver–vehicles on a homogeneous road could have different average speeds at a given density (Treiber and Kesting, 2013). The heterogeneity of traffic environments, road conditions, vehicles, drivers, and driving behaviors and dynamic instabilities of traffic flow produce wide scattering in empirical speed–density or flow–density plots, which indicates that the mean speeds or flow rates that correspond to each density vary substantially over a finite range rather than remaining fixed (Coifman, 2015; Daganzo, 2002; Dong et al., 2015; Kerner, 2009; Laval et al., 2006; Nishinari et al., 2003; Tang et al., 2011; Treiber and Helbing, 1999; Treiber et al., 2006; Treiber and Kesting, 2013; Windover and Cassidy, 2001).

Therefore, various stochastic structures have been proposed to represent uncertainty of traffic flow during FD modeling (Qian et al., 2017; Qu et al., 2017; Siqueira et al., 2016). Most studies have focused on headway distribution, allowing different headway values to correspond to one speed (Chen et al., 2014; Ghiasi et al., 2017; Li and Chen, 2017). Most of the previous studies assumed headway distributions with respect to the mean speed as position-dependent or state-dependent log-normal distributions under given speed ranges around an expected value. It implies that all headways for a position or a steady state within a given speed range were assumed to follow a certain log-normal distribution. They estimated the speed-dependent flow rate distribution based on the probability distribution of headways within a given speed range, and finally derived the joint probability functions of flow and density with the use of car-following models or cellular automaton (Jabari and Liu, 2012, 2013; Jabari et al., 2014; Li and Chen, 2017; Ossen and Hoogendoorn, 2011; Sumalee et al., 2011). Some other studies have identified the time gap as a random variable to establish stochastic traffic flow models in which the time gap was assumed to follow a Log-normal, Gamma, or Weibull distribution, and the modeling approach based on time gap is similar to that based on headway (Kim and Zhang, 2008; Tordeux et al., 2010; Wu and Liu, 2013). All these stochastic FDs can explain the scattering features of flow–density plots from the microscopic perspective.

However, these headway- or time gap-based models rely on the assumption of a specific distribution for microscopic variables that varies with traffic environments, traffic conditions, vehicles, drivers, and driving behaviors. These presumed distributions may not be able to fully capture the characteristics of microscopic variables due to the heterogeneity of the empirical data. For example, the headway or time gap distributions may vary according to traffic rules and driver behaviors, or the distributions that result from different car-following types may differ due to the heterogeneity in vehicle types. In addition, most of these stochastic FDs have complicated modeling procedures, so their application in real-time traffic environment is inconvenient due to their derivation from prespecified microscopic traffic models.

Theoretically, as an alternative to derivation of the parameters from prespecified microscopic models, the stochastic FD can be calibrated directly from the empirical macroscopic traffic data. However, this method has rarely been studied. To establish a stochastic FD based on the empirical macroscopic traffic data, two core questions must be answered: How should the uncertainty of traffic flow be represented using the available variables? How should a physically reasonable and elegant formulation to incorporate random variables into traffic stream models be explored? To address the two research questions, this study aims to (a) explore a stochastic structure to incorporate the variables that represent the uncertainty into the traffic stream model; (b) establish a stochastic link-based FD under an explicit consideration of various heterogeneity effects.

The remainder of this paper is structured as follows: Section 2 explains the sources of uncertainty and the structures of a stochastic link-based FD. Section 3 describes the characteristics of real-world traffic data in Hong Kong. Section 4 presents the model specification and the methods for calibration. Section 5 presents the methods used for model comparison and validation. In Section 6, the stochastic FD is calibrated and validated using real-world traffic data from Hong Kong. In Section 7, the stochastic components of the variance of FD are discussed. Finally, concluding remarks and potential directions for future research are provided in Section 8.

2. Stochastic model under explicit consideration of speed heterogeneity

2.1. Sources of uncertainty

From a macroscopic perspective, traffic flow uncertainty can be incorporated as variance in the FD. In the speed–density relationship, the uncertainty is represented by the variance of the mean speed corresponding to a particular density. Vehicular speed exhibits an inherent random character because it depends on the heterogeneity of drivers' perceptions and responses regarding various external traffic environments and dynamic instabilities of traffic flow. Even under identical traffic environments, different drivers have different perceptions and responses, which results in various speeds. This variation is attributable to the heterogeneity of the vehicle types and drivers with varied perceptions and responses regarding identical external traffic environments.

Speed heterogeneity is a source of uncertainty and can be directly obtained using on-road detectors. With the advent of various high-tech devices, considerable high-resolution traffic data can be collected by on-road detectors installed for real-time traffic monitoring, which can continuously record and store the information of individual vehicles. By using a real-time data processing system, high-resolution macroscopic traffic data, including space mean speed and speed variance, can be readily obtained by aggregating individual vehicle data within a short time interval (e.g., 2 min). Within such a short interval, the external traffic environment can be considered nearly identical for all passing vehicles. Thus, speed variance, which is calculated as the variance of the space mean speeds of all vehicles, can represent the speed heterogeneity at an identical density under a uniform traffic environment.

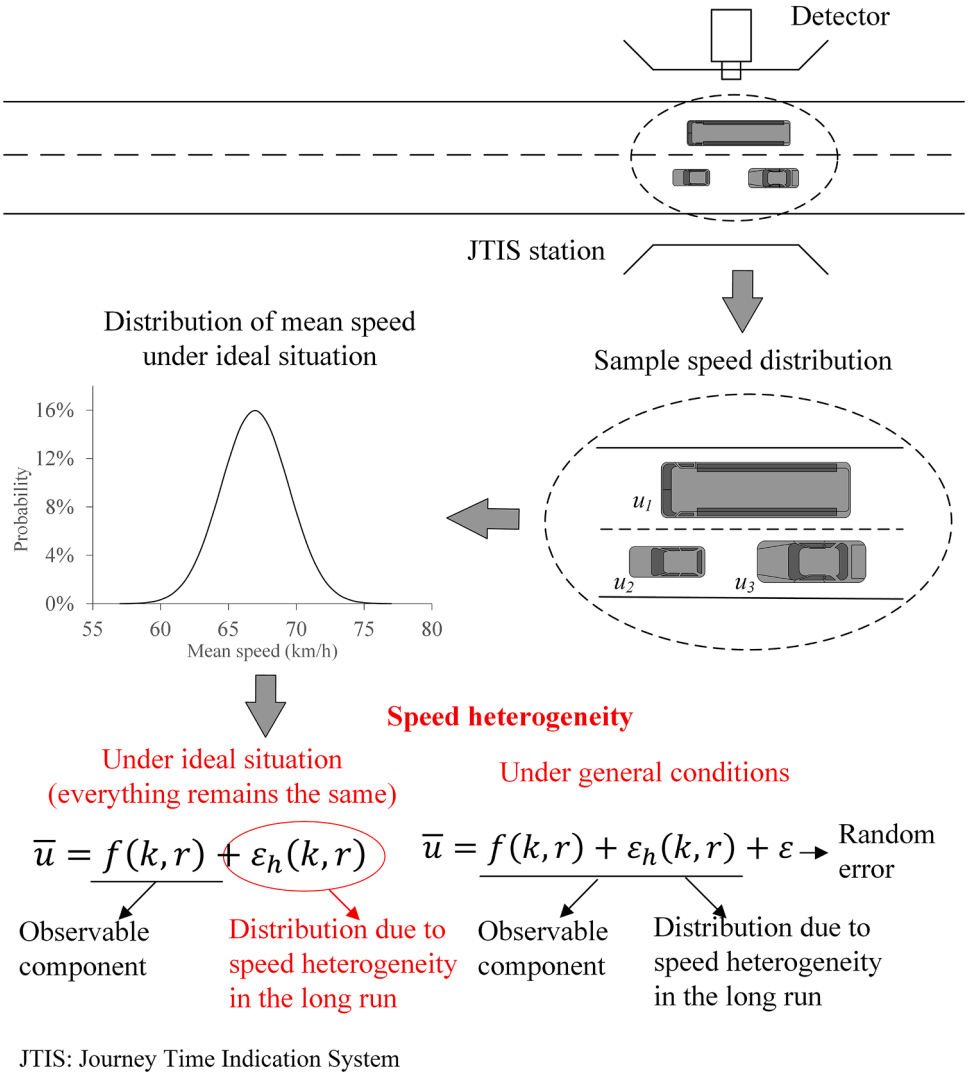

Fig. 1. Definition of speed heterogeneity.

In addition to speed heterogeneity, traffic environment is another factor influencing vehicular speed. Drivers exhibit different perceptions, responses, and driving behaviors in varied traffic environments. For example, under rainy conditions, drivers tend to reduce their speeds, which results in a lower mean speed (Lam et al., 2013). The reduced speeds largely depend on drivers' responses to the rainfall, thus influencing the speed variance. Thus, rainfall intensity which represents a kind of traffic environment is another source of uncertainty. In this study, two available sources of uncertainty are considered: (1) Speed heterogeneity at an identical density under an identical traffic environment, which is indicated by the speed variance within a short interval, and (2) rainfall intensity, which represents the traffic environment. Other than the observable heterogeneity due to speed heterogeneity and rainfall intensity, several unobservable heterogeneity may exist due to various unknown factors, such as occurrence of traffic incidents, strong prevailing wind, and sun glare effect, some of which may relate to density. Both observable heterogeneity and unobservable heterogeneity are expected to contribute to the uncertainty of traffic flow.

2.2. Ideal model considering speed heterogeneity

As shown in Fig. 1, for a given density k under an identical environmental condition where the rainfall intensity is indicated by r, an on-road detector continuously measures a sample of n vehicles from a population of passing vehicles in each short interval (e.g., 2 min) and outputs the mean speed $\overline{u}$ and speed variance $Var(u)$. Under an identical environmental condition, as all factors remain constant, if the detector repeats sampling from the population of vehicles, for a given density k and rainfall intensity r, the mean speed $\overline{u}$ will follow a distribution with a population mean μ and variance of mean speed $\sigma_h^2(k,r)$. Under an identical environmental condition with rainfall

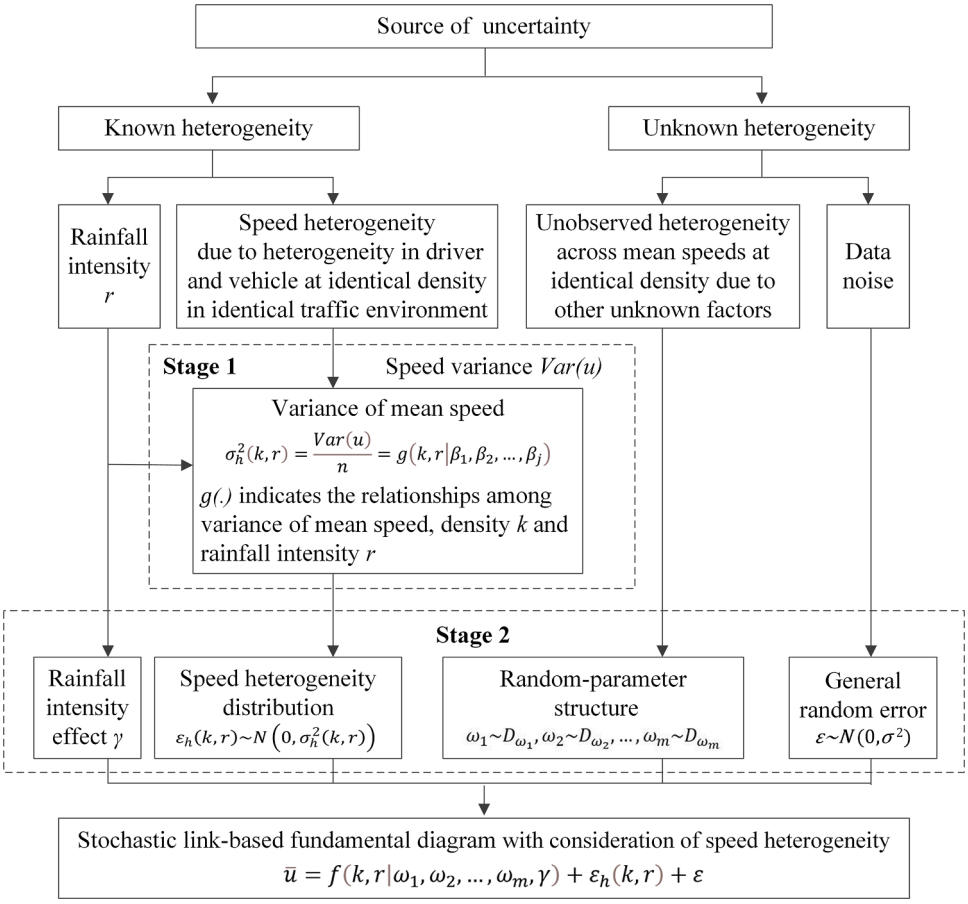

Fig. 2. Framework of stochastic link-based fundamental diagram.

intensity r, in each interval, for a given density k, the variance $\sigma_h^2(k,r)$ can be estimated as

$$\sigma_h^2(k,r) = \frac{\sigma_p^2(k,r)}{n} \tag{1}$$

where $\sigma_p^2(k,r)$ is the population variance of vehicular speed.

For a given density k, each sample outputs its own speed variance $Var(u)$, which is an unbiased estimator of population variance $\sigma_p^2(k,r)$ of vehicular speeds at density k and rainfall intensity r within the given interval. This means that in the presence of adequate samples, the long-term averages of these speed variances at k and r approach the population variance $\sigma_p^2(k,r)$. Therefore, both the population variance $\sigma_p^2(k,r)$ of vehicular speed and the variance $\sigma_h^2(k,r)$ of mean speed are dependent on k and r. Then, $\sigma_h^2(k,r)$ can be determined as

$$\sigma_h^2(k,r) = \frac{\sigma_p^2(k,r)}{n} = \frac{Var(u)}{n} = g\left(k,r\beta_1,\beta_2,\ldots,\beta_j\right) \tag{2}$$

where $g(\cdot)$ indicates the relationships among the variance $\sigma_h^2(k,r)$, density k, and rainfall intensity r, which can be estimated from the traffic data, and $\beta_1,\beta_2,\ldots,\beta_j$ are model parameters in the relationship $g(\cdot)$.

If the population mean speed in the interval is assumed to be a function of k and r (i.e., $\mu = f(k, r)$), then for a case in which all environmental factors remain constant and there is no data noise in the model, an "ideal" relationship can be obtained as

$$\begin{aligned} \bar{u} &= f(k,r) + \varepsilon_h(k,r) \text{ where } \varepsilon_h(k,r) \sim N\left(0,\sigma_h^2(k,r)\right) \\ \sigma_h^2(k,r) &= g\left(k,r\beta_1,\beta_2,\ldots,\beta_j\right) \end{aligned} \tag{3}$$

where $\varepsilon_h(k,r)$ is assumed as a normal distribution due to the speed heterogeneity for given k and r. No data noise is included in the model. This model is considered ideal because even if there exists an ideal relationship among mean speed $\bar{u}$, density k, and rainfall intensity r, the expected observed speed will still follow the distribution sampled from the population of vehicles by the detector, due to

Table 1
Descriptive statistics of data.

Site	Sample size	Variable	Min.	Max.	Mean	Std.
1	254,954	$\bar{u}$ (km/h)	1.04	100.44	64.87	23.02
		k (veh/km/lane)	0.5	194.94	21.16	21.36
		r (mm/min)	0	2.50	0.0048	0.06
		$Var(u)/n$ (km/h)^2	0.05	211.16	2.78	4.08
2	243,174	$\bar{u}$ (km/h)	1.02	89.56	57.92	14.53
		k (veh/km/lane)	0.84	199.00	19.66	20.26
		r (mm/min)	0	2.50	0.0048	0.06
		$Var(u)/n$ (km/h)^2	0.06	154.09	4.53	7.64

the speed heterogeneity under an identical traffic environment.

2.3. Random-parameter model with consideration of speed heterogeneity

In general, the above ideal relationship can never be absolutely achieved, due to the presence of various unobserved heterogeneities (other than speed heterogeneity) and data noise. Therefore, a random-parameter structure with the parameters $\omega_1,\omega_2,\ldots,\omega_m$ is introduced into the relationship $\mu = f(k, r)$ to reveal the unobserved heterogeneity in the mean speeds across density k. In addition, a parameter γ is used to represent the effect of rainfall intensity and a general random error is added in Eq. (3) to represent the effects of data noise. Fig. 2 presents the framework of the random-parameter model with consideration of speed heterogeneity (RPWSH).

Based on above ideal relationship, a complete model under general conditions can be obtained as

$$\begin{aligned} &\bar{u} = f(k, r\omega_1,\ \omega_2, \ldots, \omega_m, \gamma) + \varepsilon_h(k, r) + \varepsilon \\ &\text{where } \omega_1 \sim D_{\omega_1},\ \omega_2 \sim D_{\omega_2}, \ldots, \omega_m \sim D_{\omega_m}, \varepsilon_h(k, r) \sim N\left(0, \sigma_h^2(k, r)\right),\ \varepsilon \sim N\left(0, \sigma^2\right) \end{aligned} \tag{4}$$

where $f(\cdot)$ indicates the relationship among mean speed, density, and rainfall intensity; $\omega_1,\omega_2,\ldots,\omega_m$ are random parameters, and D_{ω_1}, $D_{\omega_2},\ldots, D_{\omega_m}$ are their distributions, respectively; γ is the effect of rainfall intensity; and ε is a general random error resulting from the data noise, which is assumed to be normally distributed with a mean of zero and variance of σ^2. In RPWSH, $f(\cdot)$, $\sigma_h^2(k,r)$ and D_{ω_1}, $D_{\omega_2},\ldots,$ D_{ω_m} can be determined from the traffic data.

3. Data collection and processing

Here, two case studies were conducted in Hong Kong to illustrate the procedure for calibrating the proposed stochastic FD. A metropolitan area located in the eastern Pearl River Delta of the South China Sea, Hong Kong is one of the most densely populated cities globally, with a total area of approximately 1,100 km^2. The population is multi-national and exceeded 7.4 million in mid-2019. The Hong Kong government possesses complete high-quality datasets, thus making the multisource high-resolution data, such as those related to traffic flow, speed, and weather, available for this study.

Our traffic data were obtained from the Hong Kong Journey Time Indication System (JTIS) operated by the Hong Kong Transport Department. The JTIS provides the average journey time estimates for several major routes in Hong Kong with an updated interval of every 2 min (Lam et al., 2013). Autoscope video traffic detectors were installed at the major roads in Hong Kong to collect real-time traffic data, such as space mean speed, its variance, and traffic count. Two road sections were selected for the case studies: one at Gloucester Road westbound, a major urban three-lane expressway, and the other at Victoria Park Road westbound, an urban two-lane road. The traffic data were collected at 2-min intervals from January 1 to December 31, 2017.

The mean speed $\bar{u}$, speed variance $Var(u)$, and traffic count n in the 2-min intervals on the two selected traffic lanes were obtained using traffic detectors. The variance of mean speed due to speed heterogeneity was calculated from $Var(u)/n$. As the traffic density data were not available from the JTIS traffic detector dataset, the traffic density k on a per-lane basis was derived from the following Eqs. (5)–(7):

$$k = \frac{1}{n_{lane}} \times \frac{n \times 30}{\bar{u}} \tag{5}$$

where n_{lane} is the number of lanes in the selected road sections. As explained above, within each interval, all factors remained constant. Due to the speed heterogeneity, the mean speed $\bar{u}$ follows a distribution with mean μ and variance $\sigma_h^2(k,r)$. Considering a Taylor series expansion of Eq. (5), we approximate the density k using a quadratic polynomial for k around the point $\bar{u} = \mu$, as follows:

$$k = \frac{30n}{n_{lane}} \times \left(\frac{1}{\mu} - \frac{1}{\mu^2}(\bar{u} - \mu) + \frac{1}{\mu^3}(\bar{u} - \mu)^2\right) \tag{6}$$

The mean speed $\bar{u}$ and speed variance $Var(u)$ in the dataset are the unbiased estimations of population mean μ and population variance $\sigma_p^2(k,r)$, respectively. Based on the expectation of Eq. (6), we have

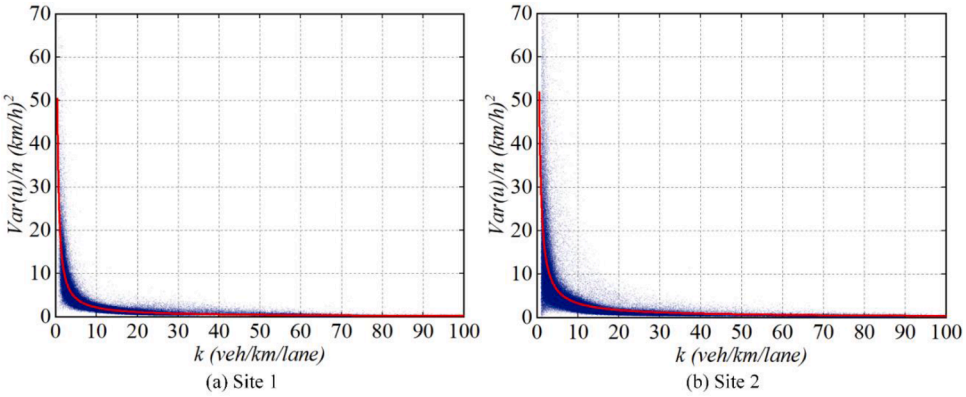

Fig. 3. Relationship between variance due to speed heterogeneity and density.

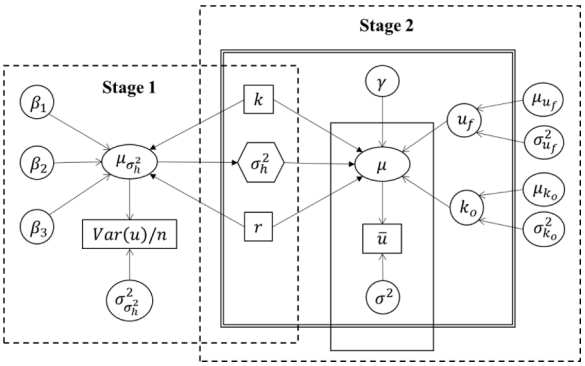

Fig. 4. Bayesian graph for the random-parameter model with consideration of speed heterogeneity

$$E(k) = \frac{30n}{n_{lane}} \times \left(\frac{1}{\mu} + \frac{\sigma_h^2(k,r)}{\mu^3}\right) = \frac{30n}{n_{lane}} \times \left(\frac{1}{\bar{u}} + \frac{Var(u)}{n\bar{u}^3}\right) \tag{7}$$

The rainfall intensity r is the rainfall precipitation during a certain period. The rainfall intensity per minute during January 1 to December 31, 2017, was obtained from the Hong Kong Observatory. The average rainfall intensity on a per-minute basis was determined by averaging the rainfalls in the 2-min interval to represent the environmental condition within the interval.

First, the raw data were filtered to ensure data validity and the outlier observations due to the malfunction of the traffic detectors were eliminated. Then, all observations with traffic count smaller than five were eliminated because of their unreliability. Similarly, the corresponding traffic datasets of rainfall intensity data with incomplete records (of which there were 370) were removed. After this data cleaning, our dataset finally comprised 254,954 observations in site 1 and 243,174 observations in site 2. The descriptive statistics of the field data are summarized in Table 1.

4. Model specification and calibration

4.1. Model specification

To establish RPWSH, the relationships $\sigma_h^2(k,r) = g(k,r|\beta_1,\beta_2,\cdots,\beta_j)$, $\mu = f(k, r|\omega_1,\omega_2,\ldots,\omega_m,\gamma)$ and the distributions $D_{\omega_1}, D_{\omega_2},\ldots, D_{\omega_m}$ need to be specified based on real-world traffic data. Accordingly, the formulation of RPWSH is specified in the following subsections.

4.1.1. Variance due to speed heterogeneity

Fig. 3 illustrates the relationship between the estimated variance $Var(u)/n$ and density k. As indicated by the red solid lines in Fig. 4, the relationship between the variance $\sigma_h^2(k,r)$ and density k can be modeled by a negative power function. Therefore, $g(\cdot)$ is defined as

$$g(k,r|\beta_1,\beta_2,\beta_3) = \beta_1(1+\beta_2 r)k^{-\beta_3} \tag{8}$$

where β_1, β_2, and β_3 are model parameters.

4.1.2. Traffic stream model with random-parameter structure

To establish the relationship among the population mean speed μ, density k, and rainfall intensity r, we compared the goodness-of-fit of the following four traffic stream models on the traffic data obtained from the selected sites: Greenshields's model (Greenshields et al., 1935), Greenberg's model (Greenberg, 1959), Underwood's model (Underwood, 1961), and Drake's model (Drake et al., 1967). The random-parameter structure was introduced in all four models, and the parameters were assumed to follow Normal, Log-normal, Gamma, and Weibull distributions, respectively. All models were calibrated using the Bayesian hierarchical modeling approach. The results show that Drake's model with Normal distributions for the parameters in the random-parameter structure yielded the best performance in terms of goodness-of-fit and exhibited the lowest deviance information criterion (DIC) value. Therefore, the fundamental relationship among μ, k, and r and the random-parameter structure can be defined as (Drake et al., 1967)

$$\mu = u_f(1+\gamma r)\exp\left(-\frac{1}{2}\left(\frac{k}{k_o}\right)^2\right),\ \text{where } u_f \sim N\left(\mu_{u_f}, \sigma^2_{u_f}\right),\ k_o \sim N\left(\mu_{k_o}, \sigma^2_{k_o}\right) \tag{9}$$

where γ is a fixed parameter for the effect of rainfall intensity; u_f and k_o are the free-flow speed and the optimal density, respectively, both of which are assumed to be normally distributed; μ_{u_f} and $\sigma^2_{u_f}$ represent the mean and variance of u_f, respectively; and μ_{k_o} and $\sigma^2_{k_o}$ represent those of k_o.

4.1.3. Formulation of RPWSH

Combined with Eqs. (8) and (9), the formulation of RPWSH in Eq. (4) can be transformed into

$$\begin{aligned}&\bar{u} = u_f(1+\gamma r)\exp\left(-\frac{1}{2}\left(\frac{k}{k_o}\right)^2\right) + \varepsilon_h(k,r) + \varepsilon \\ &\text{where } \varepsilon_h(k,r) \sim N(0, \beta_1(1+\beta_2 r)k^{-\beta_3}), u_f \sim N\left(\mu_{u_f}, \sigma^2_{u_f}\right), k_o \sim N\left(\mu_{k_o}, \sigma^2_{k_o}\right),\ \varepsilon \sim N\left(0, \sigma^2\right)\end{aligned} \tag{10}$$

Taking a Taylor series expansion of Eq. (10), the speed–density relationship can be approximated using a quadratic polynomial near the point $(u_f = \mu_{u_f},\ k_o = \mu_{k_o})$. Applying expectation on both sides, the expectation $E(\bar{u})$ of the mean speed can be estimated as

$$E(\bar{u}) = \bar{u}\left(\mu_{u_f}, \mu_{k_o}\right) + \frac{1}{2}\frac{\partial^2 \bar{u}}{\partial u_f^2}\sigma^2_{u_f} + \frac{1}{2}\frac{\partial^2 \bar{u}}{\partial k_o^2}\sigma^2_{k_o} \tag{11}$$

where $\partial^2\bar{u}/\partial u_f^2$ and $\partial^2\bar{u}/\partial k_o^2$ are the second-order partial derivatives of $\bar{u}$ to u_f and k_o, respectively.

The total variance $Var(\bar{u})$ of the mean speed, i.e., the variance of FD, can be estimated as

$$Var(\bar{u}) = \left(\frac{\partial \bar{u}}{\partial u_f}\right)^2 \sigma^2_{u_f} + \left(\frac{\partial \bar{u}}{\partial k_o}\right)^2 \sigma^2_{k_o} + \sigma^2_h(k,r) + \sigma^2 \tag{12}$$

where $\partial\bar{u}/\partial u_f$ and $\partial\bar{u}/\partial k_o$ are the first-order partial derivatives.

Thus, the 95% confidence interval can be estimated as

$$E(\bar{u}) \pm 1.96\ \times \sqrt{Var(\bar{u})} \tag{13}$$

4.2. Two-stage calibration based on Bayesian inference

RPWSH can be considered a two-stage process for calibration. In the first stage, the variance $\sigma^2_h(k,r)$ is calibrated based on the speed variance $Var(u)$, traffic count n, density k, and rainfall intensity r in the given interval to obtain the distribution $\varepsilon_h(k,r)$. In the second stage, given $\varepsilon_h(k,r)$, the random-parameter model is calibrated to determine the parameters μ_{u_f}, μ_{k_o}, $\sigma^2_{u_f}$, $\sigma^2_{k_o}$, γ and σ^2 to obtain RPWSH.

The two-stage process of model calibration can be simultaneously achieved using Bayesian inference. Based on Bayes' theorem, Bayesian inference can incorporate more evidence and new information to update the probability for a hypothesis (Lunn et al., 2013). In the two-stage calibration, the information regarding the first-stage model is incorporated into the second-stage model at each iteration of Bayesian updating. Fig. 4 illustrates the Bayesian graph for RPWSH. The distribution of the mean $\mu_{\sigma^2_h}$ of variance $\sigma^2_h(k,r)$ is estimated in the first-stage model, and simultaneously, the estimated distribution is considered as the prior distribution of $\sigma^2_h(k,r)$ in the second-stage model. In addition, combined with the available information, Bayesian inference can be used to predict the distribution of a new unknown mean speed under a given density and rainfall intensity.

In the first stage, as the variance $\sigma^2_h(k,r)$ is estimated by $Var(u)/n$, it is assumed that

$$\frac{Var(u)}{n} \sim N\left(\mu_{\sigma^2_h}, \sigma^2_{\sigma^2_h}\right) \text{ where } \mu_{\sigma^2_h} = \beta_1(1+\beta_2 r)k^{-\beta_3} \tag{14}$$

where $\mu_{\sigma^2_h}$ is the mean of $\sigma^2_h(k,r)$ and $\sigma^2_{\sigma^2_h}$ is the variance of $\sigma^2_h(k,r)$. Bayesian modeling is used to estimate the parameters β_1, β_2, β_3 and $\sigma^2_{\sigma^2_h}$. According to Bayes' theorem, the posterior distribution $p(\beta_1, \beta_2, \beta_3,\ \sigma^2_{\sigma^2_h} \mid Var(u)/n, k, r)$ can be determined as

$$p\left(\beta_1,\beta_2,\beta_3,\sigma^2_{\sigma^2_h}\middle|\frac{Var(u)}{n},k,r\right)\propto p\left(\frac{Var(u)}{n}\middle|\beta_1,\beta_2,\beta_3,\sigma^2_{\sigma^2_h}\right)p(\beta_1)p(\beta_2)p(\beta_3)p\left(\sigma^2_{\sigma^2_h}\right) \tag{15}$$

where $p(Var(u)/n|\beta_1,\beta_2,\beta_3,\sigma^2_{\sigma^2_h})$ is the likelihood of $Var(u)/n$ (i.e., $L(\beta_1,\beta_2,\beta_3,\sigma^2_{\sigma^2_h};Var(u)/n)$), and $p(\beta_1)$, $p(\beta_2)$, $p(\beta_3)$ and $p(\sigma^2_{\sigma^2_h})$ are the prior distributions specified for β_1, β_2, β_3 and $\sigma^2_{\sigma^2_h}$, respectively.

In the second stage, the variance $\sigma^2_h(k,r)$ of the distribution $\varepsilon_h(k,r)$ is estimated by $\mu_{\sigma^2_h}$, whose distribution is the prior distribution of $\sigma^2_h(k,r)$. It is assumed that

$$\begin{aligned}&\bar{u}\sim N(\mu_{\bar{u}},\sigma^2),\ \text{where } \mu_{\bar{u}}=u_f(1+\gamma r)\exp\left(-\frac{1}{2}\left(\frac{k}{k_o}\right)^2\right)+\varepsilon_h(k,r)\\&u_f\sim N\left(\mu_{u_f},\sigma^2_{u_f}\right),k_o\sim N\left(\mu_{k_o},\sigma^2_{k_o}\right),\varepsilon_h(k,r)\sim N\left(0,\mu_{\sigma^2_h}\right)\end{aligned} \tag{16}$$

where $\mu_{\bar{u}}$ is the mean of $\bar{u}$. Bayesian hierarchical modeling is used to estimate the parameters μ_{u_f}, μ_{k_o}, $\sigma^2_{u_f}$, $\sigma^2_{k_o}$, γ and σ^2. The posterior distribution $p(\mu_{u_f},\mu_{k_o},\sigma^2_{u_f},\sigma^2_{k_o},\gamma,\mu_{\sigma^2_h},\sigma^2|\bar{u},k,r)$ is given by

$$\begin{aligned}&p\left(\mu_{u_f},\mu_{k_o},\sigma^2_{u_f},\sigma^2_{k_o},\gamma,\mu_{\sigma^2_h},\sigma^2\middle|\bar{u},k,r\right)\propto p\left(\bar{u}\middle|\mu_{u_f},\mu_{k_o},\sigma^2_{u_f},\sigma^2_{k_o},\gamma,\mu_{\sigma^2_h},\sigma^2\right)\\&\times p\left(u_f\middle|\mu_{u_f},\sigma^2_{u_f}\right)p\left(k_o\middle|\mu_{k_o},\sigma^2_{k_o}\right)p\left(\varepsilon_h(k,r)\middle|\mu_{\sigma^2_h}\right)\\&\times p(\mu_{u_f})p\left(\sigma^2_{u_f}\right)p(\mu_{k_o})p\left(\sigma^2_{k_o}\right)p(\gamma)p\left(\mu_{\sigma^2_h}\right)p\left(\sigma^2\right)\end{aligned} \tag{17}$$

where $p(\bar{u}|\mu_{u_f},\mu_{k_o},\sigma^2_{u_f},\sigma^2_{k_o},\gamma,\mu_{\sigma^2_h},\sigma^2)$ is the likelihood of $\bar{u}$, and $p(u_f|\mu_{u_f},\sigma^2_{u_f})$, $p(k_o|\mu_{k_o},\sigma^2_{k_o})$, $p(\varepsilon_h(k,r)|\mu_{\sigma^2_h})$, $p(\mu_{u_f})$, $p(\sigma^2_{u_f})$, $p(\mu_{k_o})$, $p(\sigma^2_{k_o})$, $p(\gamma)$, $p(\mu_{\sigma^2_h})$, and $p(\sigma^2)$ are the prior distributions for u_f, k_o, $\varepsilon_h(k,r)$, μ_{u_f}, $\sigma^2_{u_f}$, μ_{k_o}, $\sigma^2_{k_o}$, γ, $\mu_{\sigma^2_h}$, and σ^2, respectively.

Obtaining the complete Bayesian posterior estimates requires the specification of prior distribution. In the absence of sufficient prior knowledge, noninformative priors are assumed here to estimate parameters in the two-stage model (Congdon, 2014; Dong et al., 2020):

$$\begin{aligned}&\beta_1\sim N(0,10000),\ \beta_2\sim N(0,10000),\ \beta_3\sim N(0,10000),\ \sigma^2_{\sigma^2_h}\sim IG(0.01,0.01)\\&\mu_{u_f}\sim N(0,10000),\ \ \mu_{k_o}\sim N(0,10000),\ \sigma^2_{u_f}\sim IG(0.01,0.01),\ \sigma^2_{k_o}\sim IG(0.01,0.01)\\&\gamma\sim N(0,10000),\ \sigma^2\sim IG(0.01,0.01)\end{aligned} \tag{18}$$

where $IG(\cdot)$ indicates inverse gamma distribution.

5. Model comparison and validation

RPWSH is compared with the following three candidate models: fixed-parameter model without consideration of speed heterogeneity (FPWOSH), fixed-parameter model with consideration of speed heterogeneity (FPWSH), and random-parameter model without consideration of speed heterogeneity (RPWOSH). The effect of speed heterogeneity is considered in the model structures in FPWSH and RPWSH, but not in those in FPWOSH and RPWOSH. Therefore, speed variance data are included in the datasets used in FPWSH and RPWSH, but not in those used in FPWOSH and RPWOSH. The three candidate models are presented in Eqs. (19)–(21) below.

FPWOSH can be expressed as

$$\bar{u}=u_f(1+\gamma r)\exp\left(-\frac{1}{2}\left(\frac{k}{k_o}\right)^2\right)+\varepsilon\ \text{where}\ \varepsilon\sim N(0,\sigma^2) \tag{19}$$

where the free-flow speed u_f and optimal density k_o are considered as fixed parameters.

FPWSH (i.e., $\sigma^2_h(k,r)$) can be expressed as

$$\begin{aligned}&\bar{u}=u_f(1+\gamma r)\exp\left(-\frac{1}{2}\left(\frac{k}{k_o}\right)^2\right)+\varepsilon_h(k,r)+\varepsilon\\&\text{where}\ \varepsilon_h(k,r)\sim N(0,\beta_1(1+\beta_2 r)k^{-\beta_3}),\ \varepsilon\sim N(0,\sigma^2)\end{aligned} \tag{20}$$

Comparatively, RPWOSH can be expressed as

Table 2
Estimation results for the parameters in random-parameter model with consideration of speed heterogeneity.

Site	Variable		Mean	S.D.	2.50%	Median	97.50%
1	Stage 1	β_1	20.52	0.0303	20.47	20.52	20.58
		β_2	1.14	0.0196	1.10	1.14	1.18
		β_3	0.981	0.0014	0.979	0.981	0.984
	Stage 2	μ_{k_o} (veh/km/lane)	34.31	0.0187	34.27	34.31	34.35
		μ_{u_f} (km/h)	81.60	0.0110	81.58	81.60	81.62
		γ	-0.226	0.0021	-0.230	-0.226	-0.222
		σ^2 (km/h)^2	5.48	0.1476	5.14	5.49	5.73
		$\sigma^2_{k_o}$ (veh/km/lane)^2	18.74	0.1174	18.52	18.74	18.97
		$\sigma^2_{u_f}$ (km/h)^2	2.31	0.1585	2.05	2.29	2.68
2	Stage 1	β_1	27.40	0.0598	27.28	27.40	27.52
		β_2	1.54	0.0331	1.48	1.54	1.61
		β_3	0.923	0.0021	0.919	0.923	0.927
	Stage 2	μ_{k_o} (veh/km/lane)	42.76	0.0373	42.69	42.76	42.84
		μ_{u_f} (km/h)	67.33	0.0122	67.31	67.33	67.35
		γ	-0.240	0.0030	-0.246	-0.240	-0.234
		σ^2 (km/h)^2	1.55	0.0864	1.38	1.54	1.71
		$\sigma^2_{k_o}$ (veh/km/lane)^2	68.66	0.4003	67.86	68.67	69.44
		$\sigma^2_{u_f}$ (km/h)^2	8.38	0.1101	8.17	8.38	8.60

$$\overline{u} = u_f(1+\gamma r)\exp\left(-\frac{1}{2}\left(\frac{k}{k_o}\right)^2\right) + \varepsilon$$
$$\text{where } u_f \sim N\left(\mu_{u_f}, \sigma^2_{u_f}\right),\ k_o \sim N\left(\mu_{k_o}, \sigma^2_{k_o}\right),\ \varepsilon \sim N\left(0, \sigma^2\right) \tag{21}$$

where the free-flow speed u_f and optimal density k_o are considered as random parameters.

The four models can be calibrated using Bayesian inference, as described in the above section. The above two-stage process of model calibration is applied to estimate the FPWSH and RPWSH parameters. Without considering the effect of speed heterogeneity, FPWOSH and RPWOSH can be directly calibrated using the Bayesian modeling approach and Bayesian hierarchical modeling approach, respectively.

Two measures are used for comparing the estimated and predictive performances: DIC and mean absolute percentage error (MAPE). The DIC compares the goodness-of-fit of the Bayesian models with different numbers of parameters that are calibrated using the same dataset (Spiegelhalter et al., 2005). It can be defined as

$$\text{DIC} = D(\overline{\theta}) + 2p_D = \overline{D} + p_D \tag{22}$$

where $\overline{\theta}$ indicates the posterior means of the parameters of interest, $D(\overline{\theta})$ is the deviance of $\overline{\theta}$, p_D is the effective number of parameters in the model, and $\overline{D}$ is the posterior mean of the deviance statistics. The model with a lower DIC value is considered to perform better (Spiegelhalter et al., 2005).

In contrast, the MAPE compares the predictive accuracies of the models calibrated using different datasets, and can be defined as

$$\text{MAPE} = \frac{1}{N}\sum_{i=1}^{N}\left|\frac{E(\overline{u}) - \overline{u}}{\overline{u}}\right| \times 100\% \tag{23}$$

where $E(\overline{u})$ and $\overline{u}$ are the predicted and observed mean speeds, respectively, and N is the sample size used for model validation. To perform a robust evaluation, a K-fold cross-validation is performed to assess the predictive performance of a statistical model for an independent dataset. In this cross-validation, the original dataset is randomly partitioned into K approximately equal-sized subsets. Each subset is used in turn as the validation data for assessing the predictive performance while the remaining $K-1$ subsets are combined for calibrating the statistical model. The cross-validation process is repeated K times, and therefore, each model is calibrated and evaluated K times (Hu et al., 2020). For each model, the MAPE value is calculated in each validation, and then, the K MAPE values are averaged to obtain an overall evaluation. The model with the lowest average MAPE value is considered the best.

6. Results

6.1. Calibration results for RPWSH

As described in Section 4.2, RPWSH was calibrated using two-stage Bayesian modeling. The Markov-chain Monte-Carlo method was applied to generate samples from Bayesian posterior distributions. To ensure convergence of all parameters, the two-stage model was iterated 500,000 times, where the first 200,000 iterations were removed as burn-ins and the next 300,000 were used for parameter

Table 3
Deviance information criterion values for the four models.

Site	Without speed heterogeneity		With speed heterogeneity	
	FPWOSH	RPWOSH	FPWSH	RPWSH
1	1,526,680	1,341,350	2,667,750	2,451,440
2	1,499,360	1,498,310	2,991,380	2,432,930

Table 4
Validation results for site 1.

Validation Subset	MAPE			
	FPWOSH	FPWSH	RPWOSH	RPWSH
1	8.81%	8.77%	**8.51%**	8.53%
2	6.93%	6.90%	**6.68%**	6.71%
3	9.39%	9.33%	**9.09%**	9.11%
4	7.37%	7.34%	**7.10%**	**7.10%**
5	8.44%	8.40%	**8.19%**	8.20%
6	13.02%	12.97%	12.75%	**12.70%**
7	8.57%	8.52%	8.37%	**8.34%**
8	10.93%	10.86%	10.70%	**10.66%**
9	13.95%	13.90%	13.58%	**13.55%**
10	8.58%	8.53%	8.32%	**8.31%**
11	11.85%	11.77%	11.49%	**11.40%**
12	11.32%	11.28%	10.95%	**10.92%**
Average	9.93%	9.75%	9.64%	**9.63%**

Table 5
Validation results for site 2.

Validation Subset	MAPE			
	FPWOSH	FPWSH	RPWOSH	RPWSH
1	8.88%	8.05%	8.08%	**7.91%**
2	7.93%	**7.35%**	7.38%	7.42%
3	8.52%	7.92%	7.96%	**7.86%**
4	7.04%	6.35%	6.38%	**6.29%**
5	8.04%	**7.55%**	**7.55%**	7.59%
6	11.26%	10.32%	10.36%	**10.31%**
7	9.51%	**8.63%**	8.67%	8.66%
8	9.61%	8.86%	8.88%	**8.79%**
9	12.10%	11.46%	11.49%	**11.21%**
10	8.79%	8.43%	8.42%	**8.28%**
11	9.52%	9.30%	9.29%	**9.08%**
12	9.68%	9.63%	9.56%	**9.26%**
Average	9.24%	8.65%	8.67%	**8.55%**

estimation. Markov chains and Gelman–Rubin plots were chosen to monitor the parameter convergence. The models were established and calibrated using the freeware WinBUGS14 (Spiegelhalter et al., 2005). The Bayesian credible interval (BCI) was provided to indicate the practical significance of the examined parameters (Gelman et al., 2003). As a rule of thumb, a variable can significantly impact the mean speed if the 95% BCI of its estimated mean does not cover 0, and vice versa (Chen et al., 2015; Shaheed et al., 2016). Table 2 presents the calibration results for RPWSH for sites 1 and 2.

As shown in the table, all variables in the two-stage model were statistically significant at 95% BCI. The density and rainfall intensity had significant effects on the variance of the distribution due to speed heterogeneity. Therefore, the distribution $\varepsilon_h(k,r)$ can be obtained as

$$\begin{aligned} \varepsilon_{h1}(k,r) &\sim N\left(0,\ 20.52\ \times (1+1.14r)k^{-0.981}\right) \\ \varepsilon_{h2}(k,r) &\sim N\left(0,\ 27.40\ \times (1+1.54r)k^{-0.923}\right) \end{aligned} \tag{24}$$

where $\varepsilon_{h1}(k,r)$ and $\varepsilon_{h2}(k,r)$ are the distributions resulting from speed heterogeneity for sites 1 and 2, respectively.

The mean of the free-flow speed was 81.60 and 67.33 km/h for sites 1 and 2, respectively. These calculated means were consistent with the data measured in the field. The mean of the optimal density was 34.31 and 42.76 veh/km/lane for sites 1 and 2, respectively. The variances of free-flow speed and optimal density were significant, suggesting the existence of unobserved heterogeneity across the mean speed under an identical density. The rainfall intensity had a significant and negative impact on the mean speed for sites 1 and 2.

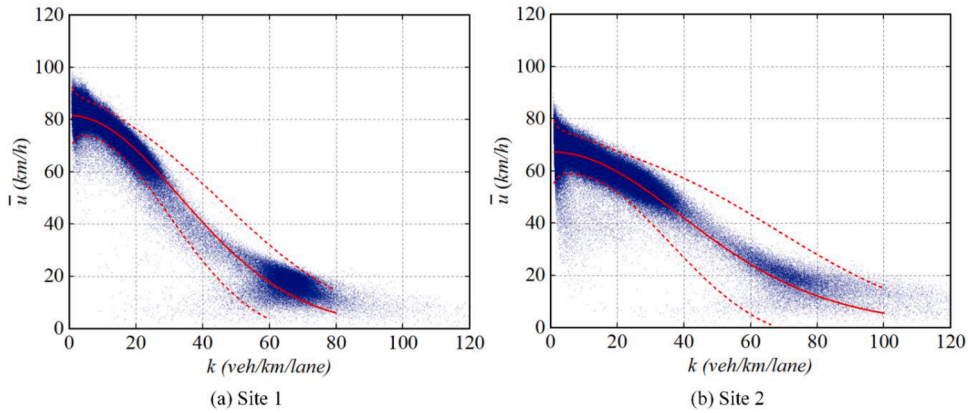

Fig. 5. Stochastic fundamental diagrams for general conditions ($r = 0$ mm/min).

6.2. Results of model comparison and validation

As described in Section 5, RPWSH was compared with FPWOSH, FPWSH, and RPWOSH. Here the effect of speed heterogeneity was considered in FPWSH and RPWSH, whereas the random-parameter models were considered in RPWOSH and RPWSH. According to the DIC results in Table 3, compared with FPWOSH and FPWSH, RPWOSH and RPWSH had lower DIC values, indicating that the random-parameter models better explain the unobserved heterogeneity in the mean speed across densities than the fixed-parameter models.

In the *K*-fold cross-validation, *K* was chosen as 12. Then, for each site, the overall dataset was divided into 12 approximately equal subsets (11×21, $246 + 1 \times 21$, 248 for site 1 and 11×20, $264 + 1 \times 20$, 270 for site 2). The traffic data available in 11 of the 12 datasets were combined for calibrating the four models, and those in the remaining dataset were used for evaluating the predictive performance of the candidate models. The MAPE values were calculated in each model's validation, and then averaged to obtain the overall results. Tables 4 and 5 present the cross-validation results for sites 1 and 2, respectively.

RPWSH had the lowest average MAPE value, indicating that the random-parameter model considering the effect of speed heterogeneity exhibits the best predictive accuracy among the four models. Moreover, FPWSH and RPWSH had lower average MAPE values than FPWOSH and RPWOSH, respectively. These results indicate that irrespective of including the random-parameter structures or not, the models considering the effect of speed heterogeneity exhibit better predictive performance. Compared with FPWOSH and FPWSH, RPWOSH and RPWSH had lower average MAPE values, respectively. These results indicate that irrespective of involving the effect of speed heterogeneity or not, the random-parameter models exhibit better predictive performance than the fixed-parameter models.

7. Discussion

This study focused on the effect of heterogeneity on the mean traffic speed at the macroscopic level. The FD can be considered as a static representation of macroscopic traffic characteristics, which focuses on the flow–speed–density relationships in a static and macroscopic sense (Jabari et al., 2014). There exist various heterogeneity sources, most of which are unobservable and cannot be quantified, although several sources can be identified with additional information. Both observable and unobservable heterogeneity can be explained in the proposed stochastic link-based FD (i.e., RPWSH). Speed heterogeneity is an observable component that can be directly obtained from the traffic data, some unobserved heterogeneity components at an identical density are identified by the random-parameter structures, and other unobservable heterogeneity components are expressed using the general random error.

The impact of heterogeneity can be expressed in terms of the variance of FD (Qian et al., 2017). In the presence of these heterogeneity effects, the variance of the parameters in Eq. (12) is expected to be statistically significant in the regression analysis. Through two-stage calibration of RPWSH, the variances of free-flow speed and optimal density, as well as the distribution resulting from the speed heterogeneity and general random error, are statistically significant in the regression analysis. These findings indicate that all abovementioned heterogeneity effects exist and contribute to the uncertainty of traffic flow.

Based on the estimated parameters, the expected mean speed, the expected variance of RPWSH and the 95% confidence interval can be calculated using Eqs. (11) – (13). Taking the rainfall intensity $r = 0$ mm/min as an example, Fig. 5 illustrates the expected mean speed with 95% confidence interval for sites 1 and 2. In the figure, the blue dots indicate traffic data in sites 1 and 2, the red solid lines represent the speed–density relationship calibrated by RPWSH, and the red dotted lines represent the upper and lower bounds at the 95% confidence interval.

7.1. Variance of RPWSH

In RPWSH, the total variance of FD is the sum of three variances, (a) the variance due to speed heterogeneity, (b) the variance due to the unobserved heterogeneity identified by the random-parameter structures and (c) the variance of the general random error. The

Fig. 6. Effect of rainfall intensity.

proportions of the three variances in the total variance of FD can be calculated using Eqs. (25)–(27).

$$P_h = \frac{\sigma_h^2(k,r)}{Var(\overline{u})} \tag{25}$$

where P_h is the proportion of variance $\sigma_h^2(k,r)$ in the total variance of FD, and $Var(\overline{u})$ is the total variance of mean speed.

$$P_u = \frac{\left(\frac{\partial \overline{u}}{\partial u_f}\right)^2 \sigma_{u_f}^2 + \left(\frac{\partial \overline{u}}{\partial k_o}\right)^2 \sigma_{k_o}^2}{Var(\overline{u})} \tag{26}$$

where P_u is the proportion of variance caused by the unobserved heterogeneity in the total variance.

$$P = \frac{\sigma^2}{Var(\overline{u})} \tag{27}$$

where P is the proportion of variance of general random error in the total variance.

As the uncertainty is expressed in terms of the total variance of FD, 64%–92% of uncertainty can be identified in RPWSH. In addition, approximately18%–24% of uncertainty can be attributed to speed heterogeneity, which is an observable component that can be directly obtained from the traffic data. Approximately 45%–69% of uncertainty is attributable to the density-dependent unobserved heterogeneity identified in RPWSH. In contrast to the constant variance of FPWOSH, the variance of RPWSH is related to the density and rainfall intensity; that is, it is density- and rainfall intensity–dependent. The variance of RPWSH contains more-complete information on density and rainfall intensity than that of FPWSH and RPWOSH because density and rainfall intensity are involved in both variances due to speed heterogeneity and unobserved heterogeneity. With the observable and identifiable information, the prediction of the mean and variance of FD becomes more reliable as the proportion of the unobservable component is reduced.

7.2. Effect of speed heterogeneity

The effect of speed heterogeneity can be explained as the uncertainty caused by diverse vehicles and various drivers with varied perceptions and responses regarding the identical traffic environment and geometric features, such as lane markings on the road for determining whether lane changing is allowed. Speed heterogeneity is indicated by the variance of vehicular speeds within a given interval. In RPWSH, the effect of speed heterogeneity is expressed by a distribution with respect to traffic density and rainfall intensity. The variance caused by speed heterogeneity decreases with an increase in density and increases with the rainfall intensity. The proportion of the variance due to speed heterogeneity in total variance of RPWSH for site 1 varies from 0.67% to 85.82% across densities, with a mean of 18.97%, and that for site 2 varies from 0.62% to 92.53%, with a mean of 23.44%.

7.3. Effect of unobserved heterogeneity

Besides speed heterogeneity, there exists unobserved heterogeneity across the mean speeds at an identical density. The effect of the unobserved heterogeneity can be explained as an uncertainty caused by other unknown factors related to density, such as occurrence of traffic incidents, strong prevailing wind, and sun glare effect, and the heterogeneity in vehicles or drivers with different perceptions, responses, and driving behaviors in varied traffic environments. In RPWSH, the effect of unobserved heterogeneity at an identical density can be expressed using the random-parameter structures in the model. The proportion of the variance due to unobserved heterogeneity in total variance of RPWSH for site 1 varies from 0.10% to 90.92% across densities with a mean of 45.91%, and that for site 2 varies from 1.02% to 97.73% with a mean of 68.54%.

7.4. Effect of rainfall intensity

Fig. 6 illustrates the calibrated speed–density relationship. The free-flow and mean speeds at the optimal density decrease with an increase in the rainfall intensity. As shown in Fig. 6, in site 1, the free-flow speed is reduced from 81.60 km/h for 0-mm/min rainfall intensity to 72.22, 62.83, 53.45, and 44.06 km/h for 0.5, 1.0, 1.5, and 2.0 mm/min rainfall intensities, respectively, and further decreased to 34.68 km/h for 2.5 mm/min rainfall intensity. In addition, the mean speed at the optimal density (34.31 veh/km/lane) is reduced from 48.70 km/h for 0-mm/min rainfall intensity to 43.10, 37.50, 31.90, and 26.30 km/h for 0.5, 1.0, 1.5, and 2.0 mm/min rainfall intensities, and further decreased to 20.70 km/h for 2.5 mm/min rainfall intensity. For site 1, the 0.5-mm/min increase in rainfall intensity reduces the free-flow speed by 9.38 km/h and the mean speed at the optimal density by 5.60 km/h. Similarly, for site 2, the 0.5-mm/min increase in rainfall intensity reduces the free-flow speed by 8.08 km/h and the mean speed at optimal density by 4.71 km/h.

7.5. Effect of data noise

In RPWSH, the effect of data noise is expressed by a general random error, including density-independent unobserved heterogeneity and random variation, as well as measurement errors. The proportion of the variance of random general error in total variance of

Table 6
Variance of general random error.

Site	FPWOSH	FPWSH	RPWOSH	RPWSH
1	23.33	21.53	5.93	5.48
2	27.84	22.17	25.60	1.55

RPWSH for site 1 varies from 8.37% to 97.87% across densities with a mean of 35.12%, and that for site 2 varies from 1.62% to 88.22% across densities with a mean of 8.02%. The variance of a general random error is associated with the accuracy of the statistical models: the smaller is the variance, the higher is the accuracy (Lunn et al., 2013; Washington, et al., 2003). Table 6 presents the variances of general random errors of FPWOSH, FPWSH, RPWOSH, and RPWSH. The variance of the general random error in RPWSH is the smallest, indicating that RPWSH has higher accuracy than FPWOSH, FPWSH, and RPWOSH.

8. Conclusion

This paper proposes a stochastic link-based FD with an explicit consideration of speed heterogeneity (i.e., RPWSH) for investigating the effects of vehicle and driver heterogeneity at an identical density under an identical traffic environment on the macroscopic relations of traffic flow. Another density-dependent unobserved heterogeneity in the mean speed is revealed using random-parameter structures. The influence of rainfall intensity is identified in the proposed model. A two-stage Bayesian inference is applied for estimating the model parameters. Through its calibration and validation using real traffic data, the proposed framework is demonstrated to perform better in terms of both goodness-of-fit and predictive accuracy.

The merits of our proposed model (i.e., RPWSH) consists of five aspects. First and foremost, the RPWSH uncovers various sources of uncertainty of link traffic flow and adequately explains the scattering phenomenon of empirical speed–density plots in a static and macroscopic sense. Second, the structures of RPWSH better capture the characteristics of traffic data, resulting in a better fit. Third, RPWSH fully contains the information of the observable and identifiable variables, which makes the calibrated free-flow speed and optimal density more reliable as the proportion of the unobservable component is reduced. Fourth, the expected mean, variance, and upper and lower limit values of the 95% confidence interval are dependent on the density and rainfall intensity. Considering the stochastic influence of density and rainfall intensity, the predictive accuracy of RPWSH for the expected mean and variance of mean speed is enhanced. Finally, the less-complicated formulations of our proposed model are more convenient for application in real-time traffic monitoring.

The proposed stochastic link-based FD will help traffic engineers implement appropriate transportation planning and management, network design, vehicle routing, and traffic control. From a theoretical perspective, the RPWSH facilitates the investigation and explanation of various observed traffic phenomena related to heavy scatters in empirical speed–density plots. From an application perspective, a reliable relationship between the parameters and the less complicated formulations of RPWSH can be applied to estimate and predict the real-time traffic state and operating speed. Combined with the additional information, such as travel time data and GPS data, the proposed stochastic FD can predict within-day and day-to-day dynamics of link-based travel times.

In RPWSH, the rainfall intensity is a weather-dependent variable that represents a traffic environment. The rainfall intensity is of particular interest due to the local conditions in Hong Kong. Owing to the humid subtropical climate in Hong Kong, which causes an annual average of about 140 rainy days with rainfall intensity of more than 2,300 mm over the past 10 years (http://www.weather.gov.hk/en/cis/dailyElement.htm#), road traffic in Hong Kong frequently suffer from the adverse weather conditions such as rainstorm and typhoon. No generality should be lost by applying the modeling framework elsewhere with a different weather feature of interest (e.g., snowfall, crosswind, storm). In addition to speed heterogeneity and rainfall intensity, many other factors contribute to the uncertainty of traffic flow, such as heterogeneity in the traffic environment, traffic conditions, road design, vehicles, and drivers with different perceptions, responses, and driving behaviors in a variety of traffic environments. In addition, the unobserved heterogeneity may exist not only in the mean of the mean speeds but also in their variance. We plan to explore the effects of other traffic environments, traffic conditions, and road designs, as well as the heterogeneity in the driver and vehicle, on the uncertainty of traffic flow. The unobserved heterogeneity in the variance of mean speeds is also worthy of further investigation.

Author Statement

Lu Bai: Methodology; Software; Validation; Formal analysis; Data Curation; Writing - Original Draft

S.C. Wong: Conceptualization; Methodology; Validation; Formal analysis; Data Curation; Writing - Review & Editing; Supervision; Project administration; Funding acquisition

Pengpeng Xu: Methodology; Software; Validation; Formal analysis; Writing - Original Draft

Andy H.F. Chow: Methodology; Writing - Review & Editing

William H.K. Lam: Conceptualization; Investigation; Resources; Methodology; Writing - Review & Editing; Supervision; Project administration; Funding acquisition

Declaration of Competing Interest

None.

Acknowledgments

The work described in this paper was supported by grants from the Research Grants Council of the Hong Kong Special Administrative Region, China (Project Nos. 17204919 and R5029-18). The second author was also supported by the Francis S Y Bong Professorship in Engineering.

References

Chen, C., Zhang, G., Tian, Z., Bogus, S.M., Yang, Y., 2015. Hierarchical Bayesian random intercept model-based cross-level interaction decomposition for truck driver injury severity investigations. Accid. Anal. Prev. 85, 186–198.
Chen, X., Li, Z., Li, L., Shi, Q., 2014. Characterising scattering features in flow-density plots using a stochastic platoon model. Transportmetrica A: Transport Science 10 (9), 820–848.
Coifman, B., 2015. Empirical flow-density and speed-spacing relationships: Evidence of vehicle length dependency. Transportation Research Part B: Methodological 78, 54–65.
Congdon, P., 2014. Applied Bayesian Modelling, 2nd ed. John Wiley & Sons, Chichester, UK.
Daganzo, C., 2002. A behavioral theory of multi-lane traffic flow. Part I: long homogeneous freeway sections. Part II: merges and the onset of congestion. Transportation Research Part B: Methodological 36 (2), 131–169.
Del Castillo, J., Benitez, F., 1995. On the functional form of the speed-density relationship. I: general theory, II: empirical investigation. Transportation Research Part B: Methodological 29 (5), 373–406.
Dong, N., Meng, F., Zhang, J., Wong, S.C., Xu, P., 2020. Towards activity-based exposure measures in spatial analysis of pedestrian–motor vehicle crashes. Accid. Anal. Prev. 148, 105777.
Dong, S., Wang, H., Hurwitz, D., Zhang, G., Shi, J., 2015. Nonparametric modeling of vehicle-type-specific headway distribution in freeway work zones. ASCE Journal of Transportation Engineering 141 (11), 05015004-1–05015004-13.
Drake, J.S., Schofer, J.L., May, A.D., 1967. A statistical analysis of speed-density hypotheses. Highway Research Record 154, 112–117.
Edie, L., 1961. Car-following and steady-state theory for noncongested traffic. Oper. Res. 9 (1), 66–76.
Gelman, A., Carlin, J.B., Stern, H.S., 2003. Bayesian Data Analysis, 3rd Edition. Chapman and Hall/CRC, Boca Raton, Fl.
Ghiasi, A., Hussain, O., Qian, Z.S., Li, X., 2017. A mixed traffic capacity analysis and lane management model for connected automated vehicles: a Markov chain method. Transportation Research Part B: Methodological 106, 266–292.
Greenberg, H., 1959. An analysis of traffic flow. Oper. Res. 7, 79–85.
Greenshields, B.D., Bibbins, J.R., Channing, W.S., Miller, H.H., 1935. A study in highway capacity. Highway Research Board Proceedings 14, 448–477.
Hu, X., Leng, J., Hou, Q., Zheng, L., Zhao., L., 2020. Assessing the explanatory and predictive performance of a random parameters count model with heterogeneity in means and variances. Accid. Anal. Prev. 147, 105759.
Jabari, S.E., Liu, H.X., 2012. A stochastic model of traffic flow: theoretical foundations. Transportation Research Part B: Methodological 46, 156–174.
Jabari, S.E., Liu, H.X., 2013. A stochastic model of traffic flow: Gaussian approximation and estimation. Transportation Research Part B: Methodological 47, 15–41.
Jabari, S.E., Zheng, J., Liu, H.X., 2014. A probabilistic stationary speed–density relation based on Newell's simplified car-following model. Transportation Research Part B: Methodological 68, 205–223.
Ji, Y., Daamen, W., Hoogendoorn, S., Qian, X., 2010. Investigating the shape of the macroscopic fundamental diagram using simulation data. Transp. Res. Rec. 2161, 40–48.
Kerner, B.S., 2004. The Physics of Traffic: Empirical Freeway Pattern Features, Engineering Applications, and Theory. Springer, Heidelberg, Germany.
Kerner, B.S., 2009. Introduction to Modern Traffic Flow Theory and Control: The Long Road to Three-Phase Traffic Theory. Springer-Verlag, Berlin, Germany.
Kim, T., Zhang, H., 2008. A stochastic wave propagation model. Transportation Research Part B: Methodological 42 (7), 619–634.
Lam, W.H.K., Tam, M.L., Cao, X., Li, X., 2013. Modeling the effects of rainfall intensity on traffic speed, flow, and density relationships for urban roads. J. Transp. Eng. 139 (7), 758–770.
Laval, J.A., Daganzo, C.F., 2006. Lane-changing in traffic streams. Transportation Research Part B: Methodological 40 (3), 251–264.
Li, L., Chen, X.M., 2017. Vehicle headway modeling and its inferences in macroscopic/microscopic traffic flow theory: a survey. Transportation Research Part C: Emerging Technologies 76, 170–188.
Lighthill, M., Whitham, G., 1955. On kinematic waves II. A theory of traffic flow on long crowded roads. Proceedings of the Royal Society A: Mathematical, Physical and Engineering Sciences 229 (1178), 317–345.
Lunn, D., Jackson, C., Best, N., Thomas, A., Spiegelhalter, D., 2013. The BUGS Book: A Practical Introduction to Bayesian Analysis. Chapman and Hall/CRC, Boca Raton, Fl.
May, A.D., 1990. Traffic Flow Fundamentals. Prentice Hall, Englewood Cliffs, NJ.
Newell, G.F., 1961. Nonlinear effects in the dynamics of car following. Oper. Res. 9 (2), 209–229.
Nishinari, K., Treiber, M., Helbing, D., 2003. Interpreting the wide scattering of synchronized traffic data by time gap statistics. Phys. Rev. E 68 (6), 067101-1–067101-4.
Ossen, S., Hoogendoorn, S.P., 2011. Heterogeneity in car-following behavior: theory and empirics. Transportation Research Part C: Emerging Technologies 19 (2), 182–195.
Pipes, L.A., 1967. Car following models and the fundamental diagram of road traffic. Transp. Res. 1, 21–29.
Qian, W.L., Siqueira, A.F., Machado, R.F., Lin, K., Grant, T.W., 2017. Dynamical capacity drop in a nonlinear stochastic traffic model. Transportation Research Part B: Methodological 105, 328–339.
Qu, X., Zhang, J., Wang, S., 2017. On the stochastic fundamental diagram for freeway traffic: model development, analytical properties, validation, and extensive applications. Transportation Research Part B: Methodological 104, 256–271.
Richards, P., 1956. Shock waves on the highway. Oper. Res. 4 (1), 42–51.
Shaheed, M.S., Gkritza, K., Garriquiry, A.L., Hallmark, S.L., 2016. Analysis of occupant injury severity in winter weather crashes: a fully Bayesian multivariate approach. Analytic Methods in Accident Research 11, 33–47.
Siqueira, A.F., Peixoto, C.J.T., Wu, C., Qian, W.L., 2016. Effect of stochastic transition in the fundamental diagram of traffic flow. Transportation Research Part B: Methodological 87, 1–13.
Spiegelhalter, D.J., Thomas, A., Best, N., Lunn, D., 2005. WinBUGS User Manual. MRC Biostatistics Unit, Cambridge, UK.
Sumalee, A., Zhong, R., Pan, T., Szeto, W., 2011. Stochastic cell transmission model (SCTM): a stochastic dynamic traffic model for traffic state surveillance and assignment. Transportation Research Part B: Methodological 45 (3), 507–533.
Tang, T., Li, C., Huang, H., Shang, H., 2011. A new fundamental diagram theory with the individual difference of the driver's perception ability. Nonlinear Dyn. 67 (3), 2255–2265.
Treiber, M., Helbing, D., 1999. Macroscopic simulation of widely scattered synchronized traffic states. Journal of Physics A 32 (1), L17–L23.
Treiber, M., Kesting, A., Helbing, D., 2006. Understanding widely scattered traffic flows, the capacity drop, and platoons as effects of variance-driven time gaps. Phys. Rev. E 74 (1), 016123-1–016123-10.
Treiber, M., Kesting, A., 2013. Traffic Flow Dynamics. Springer, Heidelberg, Germany.
Tordeux, A., Lassarre, S., Roussignol, M., 2010. An adaptive time gap car-following model. Transportation Research Part B: Methodological 44 (8-9), 1115–1131.
Underwood, R.T., 1961. Speed, volume, and density relationship: quality and theory of traffic flow. Yale Bureau of Highway Traffic, pp. 141–188.

Van Aerde, M., 1995. Single regime speed-flow-density relationship for congested and uncongested highways. In: Proceedings of the 74th TRB Annual Conference. Washington, D.C., 950802. January 27, 1995.
Wang, H., Li, H., Chen, Q., Ni, D., 2011. Logistic modeling of the equilibrium speed-density relationship. Transportation Research Part A: Policy and Practice 45, 554–566.
Washington, S., Karlaftis, M., Mannering, F., 2003. Statistical and Econometric Methods for Transportation Data Analysis. Chapman and Hall/CRC, Boca Raton, Fl.
Windover, J.R., Cassidy, M.J., 2001. Some observed details of freeway traffic evolution. Transportation Research Part A: Policy and Practice 35 (10), 881–894.
Wu, N., 2002. A new approach for modelling of fundamental diagrams. Transportation Research Part A: Policy and Practice 36 (10), 867–884.
Wu, X., Liu, H.X., 2013. The uncertainty of drivers' gap selection and its impact on the fundamental diagram. Procedia - Social and Behavioral Sciences 80, 901–921.
Zhang, H., Kim, T., 2005. A car-following theory for multiphase vehicular traffic flow. Transportation Research Part B: Methodological 39 (5), 385–399.